HHS Public Access

Author manuscript

J Appl Microbiol. Author manuscript; available in PMC 2023 December 01.

Published in final edited form as:

J Appl Microbiol. 2022 December ; 133(6): 3755–3767. doi:10.1111/jam.15812.

Efficacy and Toxicity of Hydrogen Peroxide Producing Electrochemical Bandages in a Porcine Explant Biofilm Model

Gretchen Tibbits[a], **Abdelrhman Mohamed**[a], **Suzanne Gelston**[a], **Laure Flurin**[b], **Yash S. Raval**[b], **Kerryl Greenwood-Quaintance**[b], **Robin Patel**[b,c], **Haluk Beyenal**[a,*]

[a]The Gene and Linda Voiland School of Chemical Engineering and Bioengineering, Washington State University, Pullman, WA, USA

[b]Divison of Clinical Microbiology, Mayo Clinic, Rochester, Minnesota, USA

[c]Division of Infection Diseases, Mayo Clinic, Rochester, Minnesota, USA

Abstract

Aims: Effects of H_2O_2 producing electrochemical-bandages (e-bandages) on methicillin-resistant *Staphylococcus aureus* (MRSA) colonization and biofilm removal were assessed using a porcine explant biofilm model. Transport of H_2O_2 produced by the e-bandage into explant tissue and associated potential toxicity were evaluated.

Methods and Results: Viable prokaryotic cells from infected explants were quantified after 48 h treatment with e-bandages in three *ex vivo S. aureus* infection models: 1) reducing colonization, 2) removing young biofilms, and 3) removing mature biofilms. H_2O_2 concentration-depth profiles in explants/biofilms were measured using microelectrodes. Reductions in eukaryotic cell viability of polarized and non-polarized noninfected explants were compared. E-bandages effectively reduced *S. aureus* colonization (P=0.029) and reduced the viable prokaryotic cell concentrations of young biofilms (P=0.029) and had limited effect on mature biofilms (P>0.1). H_2O_2 penetrated biofilms and explants and reduced eukaryotic cell viability by 32–44% compared to non-polarized explants.

Conclusions: H_2O_2 producing e-bandages were most efficacious when used to reduce colonization and remove young biofilms rather than to remove mature biofilms.

*Corresponding author: beyenal@wsu.edu.

Author contributions

GT, AM, SG, LF, YR, KGQ, RP, and HB developed the explant model. GT and SG performed the explant processing and e-bandage experiments. GT and AM performed microelectrode measurements. GT wrote the initial draft. HB and RP acquired the funding. GT, AM, SG, LF, YR, KGQ, RP and HB participated in writing the manuscript.

Conflict of interest

H.B. holds a patent (US20180207301A1), “Electrochemical reduction or prevention of infections,” which refers to the electrochemical scaffold described herein. R.P. reports grants from ContraFect, TenNor Therapeutics Limited, and BioFire. R.P. is a consultant to Curetis, Specific Technologies, Next Gen Diagnostics, PathoQuest, Selux Diagnostics, 1928 Diagnostics, PhAST, Torus Biosystems, Day Zero Diagnostics, Mammoth Biosciences, CARB-X, and Qvella; monies are paid to Mayo Clinic. Mayo Clinic and R.P. have relationships with Adaptive Phage Therapeutics and Pathogenomix. R.P. is also a consultant to Netflix. In addition, R.P. has a patent on *Bordetella pertussis/parapertussis* PCR issued, a patent on a device/method for sonication with royalties paid by Samsung to Mayo Clinic, and a patent on an anti-biofilm substance issued. R.P. receives honoraria from the NBME, Up-to-Date and the Infectious Diseases Board Review Course.

Significance and Impact of Study: The described e-bandages reduced *S. aureus* colonization and young *S. aureus* biofilms in a porcine explant wound model, supporting their further development as an antibiotic-free alternative for managing biofilm infections.

Keywords

Biofilm; *Staphylococcus aureus* ; electrochemical bandage; hydrogen peroxide; porcine explant; electroceutical

Introduction

A 2018 retrospective analysis estimated around 8.2 million people suffered from chronic wounds in the United States (Sen 2019). A wound that has not progressed through the normal healing stages is categorized as chronic and is often plagued with repeated infection (Sen 2019). Such wound infections are characteristically difficult to treat and often require antibiotic therapy and/or physical debridement. Chronic wound infections frequently harbor microorganisms in a biofilm form, in which an extracellular matrix is present, aiding in bacterial survival and tolerance to stresses. The structure and chemical microenvironment of a biofilm aid pathogen survival, delay wound healing, and hinder antibiotic treatment efficacy (Dowd et al. 2011; Percival et al. 2012; Metcalf and Bowler 2013). Biofilms have been found to tolerate 10–1000 times higher concentrations of many antibiotics than planktonic bacteria (Gupta et al. 2016; Uruen et al. 2021). Effective management of biofilms formed on wound surfaces could promote wound healing and prevent reinfection.

Antibiotics are a strategy for removing biofilms from infected wounds. However, extracellular polymeric substance (EPS) in biofilms restrict the activity of many antibiotics by limiting transport into the biofilm (Stewart 1996; Anderl et al. 2000), providing sites for interactions and absorption to biomolecules inside the EPS (Davenport et al. 2014), supporting cell-to-cell communication (Shrout et al. 2011), and contributing to intrinsic antibiotic tolerances (Høiby et al. 2011). As biofilms grow, maturity leads to coordinated quorum sensing and signaling pathways, exosome cell-to-cell communication (Valadi et al. 2007; Kowal et al. 2014), extracellular DNA (Devaraj et al. 2019), and increased cell numbers. Communication pathways allow cells to signal environmental changes and activate survival mechanisms. Therefore, it is expected that mature biofilms are more resistant to antibiotics or biocides.

Natural biocides are products of host immune response to infection and as such, wound healing (Hampton et al. 1998; Halliwell et al. 2000a). A common biocide is hydrogen peroxide (H_2O_2). The use of H_2O_2 in the treatment of wound biofilms is hampered by its short half-life, instability in wound beds, and toxicity to host tissue when used at high concentrations (>50 μmol L^{-1}, depending on the exposure location) (Halliwell et al. 2000a). Our team is developing an electrochemical system for continuous generation of H_2O_2 for preventing and treating wound infections (Sultana et al. 2015; Raval et al. 2019; Raval et al. 2020). H_2O_2 is an oxidizing agent that causes membrane depolarization, oxidizes proteins, and inhibits enzyme activity, resulting in cell death (Finnegan et al. 2010). The electrochemical system continuously

generates H_2O_2 from partial reduction of dissolved oxygen through the reaction, $O_2 + 2H^+ + 2e^- \leftrightharpoons H_2O_2$ ($\Delta E^{0'} = +85\ mV \frac{Ag}{AgCl},\ pH7$) generated at 0.085 $V_{Ag/AgCl}$ (Allen J. Bard 2001; Sultana et al. 2015). An electrochemical scaffold (e-scaffold) prototype, which allowed facile study of electrochemical reactions, reduced *in vitro* biofilms and explant biofilms in liquid media (Sultana et al. 2015; Sultana et al. 2016; Raval et al. 2019; Raval et al. 2020). Substition of a hydrogel for the liquid medium was used to transform e-scaffolds into electrochemical bandages (e-bandages) for direct application to wound surfaces. The e-bandage reduced *in vitro* biofilms of mono-, and dual-species microorganisms including methicillin-resistant *S. aureus*, multidrug-resistant *A. baumannii*, and yeast isolates (Mohamed et al. 2021; Raval et al. 2021b; Raval et al. 2022).

As a result of their low cost, high accessibility, and structural similarity to human dermis, porcine explants are utilized as a model for wound healing, assessing wound biofilms, and treatment efficacy (Sullivan et al. 2001). *Ex vivo* porcine models have been used to study bacteria-tissue interactions (Yang et al. 2013; Roberts et al. 2019), activity of antimicrobial agents (Lone et al. 2015; Phillips et al. 2015; Yang et al. 2017; Roberts et al. 2019; Roche et al. 2019), and cytotoxicity of treatments (Sultana et al. 2015). Here, porcine explants were used to study the efficacy, toxicity, and transport of H_2O_2 produced by e-bandages. Microbial colonization, alongside young and mature biofilm removal were tested.

Materials and Methods

H_2O_2 producing e-bandage

Construction and preparation of the H_2O_2 producing e-bandage was performed as previously described (Mohamed et al. 2021). The e-bandage is a three-electrode system consisting of a conductive carbon fabric (Zoltek, St. Louis, MO, Panex 30 PW-06) as the working and counter electrode, and an Ag/AgCl reference wire. H_2O_2 is produced as a result of oxygen reduction on the working electrode of the e-bandage. When the e-bandage was applied to biofilms, the working electrode always faced toward the biofilm. Titanium wires (TEMCo, Amazon.com, catalogue #RW0524) were connected to the working and counter electrodes using nylon sew snaps (Dritz, Spartanburg, SC, item #85). A Gamry Interface 1000 potentiostat connected with a Gamry ECM8 electrochemical multiplexer (Gamry Instruments, Warminster, PA) was used to polarize the working electrode at −0.6 $V_{Ag/AgCl}$ to generate H_2O_2. Before use, e-bandages were autoclaved (15 min at 121°C).

Chemicals, supplies, and bacteria

Dulbecco's Modified Eagle Medium (DMEM) (Thermo Fisher Scientific, #21063029) and 100X antibiotic-antimycotic (10,000 units ml^{-1} penicillin, 10,000 μg ml^{-1} streptomycin, and 25 μg ml^{-1} amphotericin B, ThermoFisher, cat. no. 15240096), and tryptic soy broth (TSB, BD Ref. 211825) were used as purchased. Phosphate buffer saline (PBS) solution contained 0.01 mol L^{-1} Na_2HPO_4, 1.8 mmol L^{-1} KH_2PO_4, 0.137 mol L^{-1} NaCl, and 2.7 mmol L^{-1} KCl and was autoclaved prior to use (15 min at 121°C). Hydrogel was prepared by dissolving 1.8 wt % sterile xanthan gum (Namaste Foods LLC, Coeur d'Alene, ID) in 500 ml of sterile PBS. Three types of tryptic soy agar (TSA, BD Ref. 236950) plates were used. 1.8 wt % TSA was used for CFU quantification before and after treatments,

1X antimcirobial agent (10 units ml^{-1} penicillin, 10 μg ml^{-1} streptomycin, and 0.025 μg ml^{-1} amphotericin B) TSA plates for cell viability measurements, and 0.1X antimicrobial agent (1 unit ml^{-1} penicillin, 1 μg ml^{-1} streptomycin, and 0.0025 μg ml^{-1} amphotericin B) TSA plates for infection experiments. 700 ml of 1.8 wt % TSA was autoclaved and allowed to cool to 45°C. 1X and 0.1X plates were prepared by adding 200 μl or 20 μl of stock antimicrobial agent solution, respectively, to 20 ml of TSA and poured into individual Petri dishes. When not in use, TSA plates were stored at 4°C. A clinical isolate of methicillin-resistant *S. aureus* (IDRL-6169) was used for all experiments.

E-bandage assessments

E-bandages were tested to assess efficacy, toxicity, and transport of H_2O_2 into explants (Figure 1). Three *S. aureus* infection models were used—colonization, and young and mature biofilms—to quantify antimicrobial effects and noninfected explants used to study toxicity. All treatment durations were 48 h and all experiments included polarized, non-polarized e-bandages and no e-bandage. For infection colonization experiments, explants were inoculated with *S aureus* and treatment started right away. Young biofilms were allowed to establish for 24h before starting treatment, and mature biofilms were allowed to establish for three days before starting treatment. Eukaryotic cell toxicity was assessed absent infection.

Explant agar biofilm model

The experimental procedure is summarized in Figure 1. Infected and noninfected models of porcine explants began with surgically scrubbing (Fig 1.1) and shaving off hair from a fresh pig ear (Fig 1.2). The outer edge of the ear was cut off with a sterile scalpel (Fig 1.3) and the epidermis layer removed with a sterile Padgett's dermatome (Nouvag TCM 3000) (Fig 1.4). A 500-μm slice of the dermis was cut. Then, a 5-mm biopsy punch (Robbins Instruments Part No. RBP-50) was used to punch 5-mm sections of the tissue (Fig 1.5). For the noninfected model (Fig 1.6A), a 5-mm explant was placed onto a 13-mm polycarbonate membrane (Cytivia Life Sciennces, 10417001) on a 1X antimicrobial agent TSA plate (Fig 1.7A). One hundred μl of hydrogel was added to the explant. Then the e-bandage was soaked in PBS and 100 μl of hydrogel added inside the e-bandage. The e-bandage was placed on the noninfected explant, and 100 μl of hydrogel added on top of the e-bandage (Fig 1.8A). The e-bandage was covered with Tegaderm™ (3M, 16002) and connected to a potentiostat to operate the e-bandage, and (Fig 1.9A) finally a PrestoBlue cell viability assay (ThermoFisher, cat. no. A13261) was performed after treatment. For the infected model (Fig 1.6B) a 5-mm explant was placed onto a 13-mm polycarbonate membrane on a 0.1X antimicrobial agent TSA plate and inoculated with bacterial (Fig 1.7B) and 100 μl of hydrogel was added on top of the infected explant. The e-bandage was soaked in PBS, 100 μl of hydrogel added to the inside layers of the e-bandage, the e-bandage placed on top of the infected explant, and 100 μl of hydrogel added on top of the e-bandage. (8B) The e-bandage was covered with Tegaderm™ and connected to a potentiostat to operate the e-bandage, and finally (9B) quantification of biofilm was done by serial dilution after treatment. The detailed protocol can be found in SI Section 3 (Detailed Explant Preparation Protocol).

Porcine explant preparation

Porcine explant preparation was modified from previous explant models to accommodate an agar model (Zmuda et al. 2020). Ear tissue was harvested from fresh pigs (same day) from local butchers, immediately cooled to 4°C and transported to the laboratory for processing. The ears were scrubbed with a single-use sponge and 10% detergent under cold water (Fig 1.1). Next, the hair was removed using an electric razor and the ears rinsed with cold water. The ears were then scrubbed with betadine soap for 10 min using gauze sponges and sprayed with 70% ethanol. The ears were then placed on UV-sterilized aluminum foil in a biosafety cabinet and cleaned again using betadine solution and sterile gauze sponges for 5 min. Betadine was removed using 70% ethanol-soaked gauze sponges. This step was continued until the gauze sponges could be wiped across the surface with no discoloration of the sponge. The outer rim of the ear was then removed using a single-use sterile razor blade and cut into 3 or 4 pieces (Fig 1.2). The epidermis was removed using a dermatome set to 500 μm and discarded (Fig 1.1–3). A 500-μm layer of the dermis was removed using the dermatome for a 500-μm-thick tissue (Fig 1.1 – 4). The tissue was placed in sterile DMEM in a Petri dish. The 500-μm dermis tissue was then punched with a 5-mm sterile biopsy punch (Fig 1.1–5). A UV-sterilized 13-mm, 0.2-μm pore-size membrane was placed on a 1X antimicrobial agent TSA plate (cell viability) or 0.1X antimicrobial agent TSA plate (infection models) and the 5-mm porcine punch positioned in the center of the membrane. The infected and noninfected explants were maintained in an incubator with 5% CO_2, 95% air, and 95% relative humidity at 37°C.

Cell viability of porcine explants

For cell viability measurements, porcine explants were placed onto 13-mm, 0.2-μm pore-size membranes on 1X antimicrobial agent TSA plates and treated with e-bandages identically to the infected models, but without bacteria (Fig 1.6A – 9A). Titanium wires of the working and counter electrode and the external Ag/AgCl wire were secured around the edges of Petri dishes with tape. Tegaderm™ was used to secure the position of the e-bandage on top of the explant (Fig 1.7A and 8A). The lid was placed on the Petri dishes and secured with parafilm. Following treatment, explants were transferred to a 96-well plate with 180 μl of DMEM and 20 μl of PrestoBlue cell viability assay (Thermo Fisher, A13262). Explants were incubated for 3 h at 37°C in an incubator with 5% CO_2, 95% air, and 95% humidity, and the fluorescence measured by excitation at 535 and emission at 590 nm (Fig 1.9A, Cytation5 imaging reader, BioTek). Explant viability was normalized to initial cell viability (i.e., before treatment) and cell viability reductions by polarized e-bandages calculated as described in SI Section 1 (equations for normalized cell viability and cell viability reduction).

Staphylococcus aureus ex vivo infection model

Three models were tested for efficacy of the e-bandage on *S. aureus*: colonization, and young and mature biofilms. Frozen stock cultures were used to grow generation 2 plates from generation 1 streak colonies on blood agar for 24 h (Trypticase™ Soy Agar II with 5% sheep blood, BD™ Cat. No. 254087). A single colony of the freshly streaked bacteria on sheep blood agar was suspended in 5 ml of TSB and incubated for 2 to 2.5 h at 37°C

to achieve 7.8 ± 0.2 $\log_{10}$ CFU ml^{-1} (0.5 McFarland). For the colonization model, 10 µl of 0.5 McFarland *S. aureus* was used to inoculate fresh explants (immediately after processing), and the e-bandages were placed and polarized 10 min later (Fig 1.6B). For the colonization model, an air incubator at 37°C was used because *S. aureus* did not grow on the no e-bandage or non-polarized infected explants at room temperature; all other treatments were done at room temperature. Two biofilm types were tested: young and mature. For young biofilm model, 10 µl of 0.5 McFarland *S. aureus* was used to inoculate fresh explants and allowed to grow for 24 h. For mature biofilms, explants were inoculated with 10 or 2.5 µl of 0.5 McFarland *S. aureus* and grown on 0.1X TSA explants for 3 days in an incubator with 5% CO_2, 95% air, and 95% humidity at 37°C. Every 24 h, explants were transferred to fresh 0.1X TSA plates. E-bandages were prepared and positioned identically to those of the noninfected model (Fig 1.7B and 8B). After treatment, e-bandages were rinsed with 5 ml of PBS; PBS was combined with the infected explants and membranes and vortexed for 30 s. Then, the combined solution was sonicated in a water bath for 5 min and vortexed again for 30 s. Finally, the combined solution was centrifuged for 10 min at 5000 rpm (3490Xg), the supernatant discarded, and the bacterial cell pellet resuspended in 1 ml of fresh PBS. The resuspension was serially ten-fold diluted in PBS and spread onto TSA plates for CFU quantification (Fig 1.9B). Individual colonies on the TSA plates were quantified after 24 h of growth.

H_2O_2 concentration depth profiles in porcine explants

H_2O_2 microelectrodes were constructed similarly to those in previous work (Lewandowski and Beyenal 2013). Briefly, an etched 50-µm platinum wire (California Fine Wire Company Pure TC grade) was sealed inside a glass capillary (Corning 8161) using a healing coil. The tip of the sealed platinum wire was exposed and electroplated with platinum to form a 20–30 µm ball. The microelectrodes were then dipped in a cellulose acetate membrane and dried for 24 h. To measure H_2O_2 concentrations, the microelectrode was polarized at $0.8V_{Ag/AgCl}$ relative to an external leakless Ag/AgCl reference electrode (similar to EDAQ ET072–1). Before and after each profile, the microelectrode was calibrated using a stock solution of H_2O_2 aliquoted into PBS from 0 to 500 µmol L^{-1}. The calibration solution was stirred constantly. The sensitivity and limit of detection of the microelectrode were 0.01 nA $µmol^{-1}$ L and 14 µmol L^{-1}, respectively. The surface of the explant/biofilm was determined using a Zeiss Stemi 2000 stereomicroscope (Carl Zeiss Microscopy, Northwood, NY, USA) and a computer-controlled stepper motor (Physik Instrumente, part no. M230101SX) controlled by a LABVIEW script. This was used to move the microelectrode in 25-µm increments from 200 µm above the explant to 300 µm below the explant/biofilm surface. A G300 Gamry potentiostat was used to measure the current response of the microelectrode (Gamry Instruments, Warminster, PA, USA).

Immediately after an e-bandage was removed from a 48 h non-polarized or polarized explant (infected or noninfected), the microelectrode was positioned at the surface of the explant using a stereomicroscope. The microelectrode tip was retracted by 3 mm from the surface, and 100 µl of hydrogel added on top of the explant. The microelectrode tip was repositioned 200 µm above the surface and polarized for 3 min to measure background current.

Scanning electron microscope imaging of porcine explants

Immediately following treatment, explants were placed in 2% paraformaldehyde/2% glutaraldehyde in 0.1 M phosphate buffer and stored overnight at 4°C. To rinse the fixing solution, the explants were washed with 0.1 M phosphate buffer twice for 15 min at room temperature. Explants were dehydrated by single 15-min ethanol treatments at concentrations of 10%, 30%, 50%, 70%, and 90% followed by two 15-min treatments at 100%. Finally, explants were critical point dried (Samdri-PVT 3B) then placed onto stubs and gold sputter-coated (Sputter Coater Technics Hummer V – Gold). A scanning electron microscope FEI Apreo and an FEI Quanta 200F microscope were used to image the explants.

Statistical analysis

A two-sided Wilcoxon rank sum test was used to assess statistical differences between treatments; experiments with a P value less than 0.1 were considered significant. Due to supply limitations for pig ears, some experiments were only replicated three times. Standard deviations and means along with individual data points are presented in the figures. Triplicate experiments were performed on different days.

Results

E-bandages prevent *S. aureus* biofilm formation on explant

During the 48 h polarized treatment time, the no e-bandage and non-polarized control explant models grew to 9.4 ±0.3 $\log_{10}$ CFU cm^{-2} and 8.6 ±1.0 $\log_{10}$ CFU cm^{-2}, respectively (Fig 2). The polarized e-bandage biofilms had an average of 5.6 ±2.5 $\log_{10}$ CFU cm^{-2} (reduction of 3.0 ±2.3 $\log_{10}$ CFU cm^{-2}), a significant reduction compared to non-polarized e-bandage treatment ($P = 0.029$).

E-bandages reduce *S. aureus* cell numbers in young explant biofilms

Young biofilms reached a cell density of 7.2 ±0.3 $\log_{10}$ CFU cm^{-2} at treatment initiation. After treatment, explant biofilms with no e-bandages had a mean cell density of 8.8 ±0.4 $\log_{10}$ CFU cm^{-2}, while non-polarized controls had a mean cell density of 7.9 ±0.3 $\log_{10}$ CFU cm^{-2} (Fig 3). In contrast, after polarized e-bandage treatment, the biofilm cell density was only 2.6 ±2.2 $\log_{10}$ CFU cm^{-2} (a reduction of 5.4 ±2.0 $\log_{10}$ CFU cm^{-2}); a statistically significant reduction (P=0.029) compared to non-polarized e-bandages.

E-bandages had limited efficacy against mature *S. aureus* biofilms

No e-bandage, non-polarized and polarized explant biofilms reached cell densities of 8.9 ±0.7, 9.7 ±0.5 and 8.9 ±0.7 $\log_{10}$ CFU cm^{-2}, respectively following treatment in the 10 µl inoculum group (Fig 4A). The cell counts in the 10 µl inoculum mature *S. aureus* explant biofilms treated with polarized e-bandages were no different than those of controls (P>0.1). In contrast, in the 2.5 µl inoculum group cell densities reached 8.6 ±0.4, 9.8 ±0.2 and 9.1 ±0.3 $\log_{10}$ CFU cm^{-2} for no e-bandage, non-polarized and polarized e-bandage biofilms, respectively (Fig 4B); in this group, mature *S. aureus* explant biofilms were reduced by 0.7 ±0.2 $\log_{10}$ CFU cm^{-2} by polarized treatment (P=0.029).

Scanning electron microscopy imaging of infected and noninfected explants

Electron microscopy images of noninfected and infected explants with no e-bandages, non-polarized e-bandages, and polarized e-bandages are shown in SI Section 2. Electron microscopy images of the no e-bandage noninfected (Fig S1A and S2A) and infected (Fig S3A and S4A) explants showed well-defined dermis fibers. Sphere-shaped *S. aureus* cells were observed on the surface of infected explants. The 0-day infected explants were sparingly covered with *S. aureus* cells while the 3-day explants had greater coverage of the surface. With non-polarized e-bandage explants (Fig S1B, S2B, S3B, S4B), the dermis fibers were still well defined and additional structures were observed on the tissue surface, likely dried hydrogel remnants. Unlike tissues not exposed to e-bandages or exposed to non-polarized explants, tissues exposed to polarized e-bandage noninfected (Fig S1C and S2C) and infected (Fig S3C and S4C) showed morphological changes. The fibers appeared to be damaged and crushed together and, in some locations, a crust was observed on the tissue. When comparing *S. aureus* cells not exposed to an e-bandage or or exposed to non-polarized e-bandages, tissue exposed to polarized e-bandages had cells that appeared to rest on the surface of the tissue rather than weaving through the fibers. No morphological changes in *S. aureus* cells were observed after polarized treatment.

H_2O_2 concentration profiles

H_2O_2 was not measurable in explants immediately after processing or in non-polarized explants (Fig 5A and B), whether infected or noninfected. For infected explants, H_2O_2 was measured in hydrogel to a concentration of ~150 μmol L^{-1} (Fig 5A). After polarized e-bandage treatment, H_2O_2 was measurable inside both *S. aureus* infected and noninfected explant tissue to at least 300 μm below the surface. H_2O_2 was measured in the concentration range of 120–250 μmol L^{-1} in hydrogel and tissue of infected explants. In the noninfected but polarized group, H_2O_2 was detected in the hydrogel and explant tissue between 150 and 275 μmol L^{-1} (Fig 5B). For both infected and noninfected explant profiles, the H_2O_2 concentration decreased as the microelectrode tip moved further into the tissue.

Eukaryotic Cell Viability

There was no statistical difference between the viability of 0-day explants exposed to no e-bandages and non-polarized e-bandages ($P>0.1$). There was a 44% average reduction in normalized cell viability between 0-day explants exposed to polarized and non-polarized e-bandages, but the difference that was not statistically significant ($P>0.1$) (Fig 6A). Viability of 3-day explants exposed to polarized e-bandages decreased by 32% compared to non-polarized explant ($P=0.001$) (Fig 6B).

Discussion

Biofilm infections are difficult to treat using systemic and topical administration of antibiotics because of the rise of antibiotic-resistant microorganisms and because of biofilm-specific antibiotic tolerance. The *in situ* electrochemical generation of biocides such as H_2O_2 is a potential approach for managing wound biofilm infections. Two devices have been developed based on an electrochemical H_2O_2 concept: e-scaffolds were developed to assess activity against biofilms grown in liquid growth media, and then e-bandages

were developed to treat agar membrane (and eventually wound) biofilms. The e-scaffold demonstrated anti-biofilm efficacy against mono-, dual-, and tri-species bacterial and fungal biofilms, without significant toxicity to host tissue in an *ex vivo* porcine explant model (Sultana et al. 2015; Sultana et al. 2016; Raval et al. 2019; Raval et al. 2020; Raval et al. 2021a). In addition, it was demonstrated that H_2O_2 generation by the electrode was the dominant mechanism of action (Sultana et al. 2015). With the e-bandage, an agar membrane biofilm model was used to simulate physical properties of the wound bed and validate the technology prior to animal testing. Polarized e-bandages were shown to be active against mono- and dual-species bacterial and yeast biofilms (Raval et al. 2021b; Raval et al. 2022). In this work, validation was extented to assessment of e-bandages against *ex vivo* biofilms grown on porcine explants.

Porcine explant models were used because of the structural similarity of pig to human skin and cost-effectiveness of the materials (Sullivan et al. 2001). The use of porcine explant models for initial assessment of efficacy and toxicity of potential antibacterial agents has been reported previously. For example, agar explant models were designed to assess toxicity and efficacy of multiple wound cleansers (Roche et al. 2019; McMahon et al. 2020). A similar model was adopted in this work to test the efficacy and toxicity of the e-bandage. The concentration of agar was increased and the concentration of antibiotics varied to address specific requirements. Increasing the agar concentration provided a stronger platform for physically supporting e-bandages. Using full strength antibiotic (1X) prevented noninfected explants from being contaminated before e-bandage treatment, while 0.1X antibiotic was suitable for allowing biofilms to grow on explants but keeping the biofilm within the boundary of the polycarbonate membrane. Cleaning of porcine tissue during processing was also modified from previous literature. Tissue has often been sterilized with chlorine gas before being infected with bacteria, but it was found that a surgical cleaning procedure with betadine and ethanol was adequate to prevent contamination with other pathogens (Yang et al. 2013; Phillips et al. 2015; Roche et al. 2019). In the end, a modified explant biofilm model was used to assess e-bandage antimicrobial activity and toxicity, and transport of H_2O_2 into explant tissue.

As all *ex vivo* models are limited by tissue viability being controlled by external conditions, such as the temperature, humidity, and suspension medium, the modified explant biofilm model was likely more susceptible to external stresses than actual wounds. Natural biocides that are produced during an immune response to infection are not generated in *ex vivo* models (Halliwell et al. 2000a). Lack of immune response means that any prevention of infection or biofilm removal in the evaluated system was a result of the H_2O_2 produced by the e-bandage. The effect on colonization of the e-bandage was studied for the first time with promising results. The e-bandage prevented *S. aureus* colonization of explants (Fig 2), and was active against established young *S. aureus* biofilms (Fig 3). *S. aureus* is most susceptible to treatment during the first 24 h when it is developing a biofilm (Alves et al. 2018). The e-bandage removed 5.4 $\log_{10}$ CFU cm^{-2} of a young *S. aureus* biofilm cells. Mature biofilms were more refractory to treatment, as expected, likely because of the complex interaction between *S. aureus* and the explant. As biofilms mature, EPS content increases, cell numbers increase, and the biofilm becomes more resilant against external challenges. The activity of H_2O_2 was studied on biofilm and planktonic phenotypes of 27

isolates of eight bacterial species (Raval et al. 2021a). H_2O_2-generating e-scaffolds had reduced activity against biofilms compared to their activity against planktonic cells. A possible reason for lower efficacy against mature compared to young biofilms, is that after 3 days, *S. aureus* cells are found hundreds of micrometers below the tissue surface (Yang et al. 2013). Another study found that *S. aureus* cells burrowed several hundred micrometers into tissue and mucosa (Cantero et al. 2013; Nakatsuji et al. 2016). Although penetration of *S. aureus* cells into the dermis was not observed in all explant experiments, the action of burrowing into tissue may be a reason that mature biofilms were less affected by e-bandages than young biofilms (Lone et al. 2015). Another reason for the reduced efficacy could be nonspecific reactions between H_2O_2, the EPS, or its components. For example, H_2O_2 was found to degrade natural polysaccharides (Ofoedu et al. 2021). EPS is comprised of many other components including dead cells, proteins, and extracellular DNA (Stewart 1996; Denkhaus et al. 2007). In the absence of antibiotic therapies, the e-bandage facilitated a limited reduction of mature biofilms (Fig 4). The efficacy of the e-bandage could be due to transport of H_2O_2 into the tissue during treatment.

Several methods for measuring transport of H_2O_2 through tissue have been described. Nanosensors were used to detect H_2O_2 in *ex vivo* cells by extrapolating the reaction of H_2O_2 with Prussian white forming Prussian blue (Marquitan et al. 2016). H_2O_2 transport was also measured using the reaction of Prussian white to blue to image the explant surface (Jankovskaja et al. 2020). A synthesized H_2O_2-response analog for electrochemically monitoring H_2O_2 permeation through tissue was tested (Yik-Sham Chung et al. 2018). Other electrochemical techniques, such as microelectrodes, can be used to measure concentration profiles in explant experiments and biofilms. Microelectrode profiles for measuring changes in pH and dissolved oxygen concentrations were conducted on uninfected and *S. aureus* infected explant tissue several hundreds of microns below the surface (Lone et al. 2015). H_2O_2 concentration profiles have also been measured using microelectrodes in *P. aeruginosa* biofilms (Stewart et al. 2000). The generation of H_2O_2 by the e-bandage was verified under abiotic conditions using microelectrodes (Mohamed et al. 2021). The concentration of H_2O_2 increased as polarizing time increased, reaching local concentrations up to 320 μmol L^{-1}. In this work, microelectrodes were used to measure H_2O_2 directly above and below the surface of explants and explant biofilms (Fig 5).

Two important observations were made based on the H_2O_2 profiles. First, H_2O_2 was measured in fresh hydrogel added atop the explant after the e-bandage was removed and prior to H_2O_2 measurement. This indicates that H_2O_2 likely diffused from the explant itself following removal of the e-bandage, which shows that H_2O_2 was not bound to tissue biomolecules. Second, H_2O_2 concentration in the tissue was highest at the hydrogel-explant or hydrogel-biofilm surface (Fig 5). H_2O_2 generated by e-bandages diffuses towards the explant surface and is then transported into tissue. As the H_2O_2 permeates throughout the tissue, the concentration decreases. The decrease in concentration may be a result of hindered transport into tissue because of nonspecific reactions. Higher H_2O_2 concentrations in noninfected explants could be explained by reduced consumption of H_2O_2 due to reactions with biofilm cells, EPS and H_2O_2-degrading enzymes. H_2O_2 is expected to be consumed as biofilm is removed from the infected explant. It is expected that electrochemical H_2O_2 generation will decrease pH. However, the hydrogel contains a buffer

which is expected to limit pH changes (until buffering capacity is depleted). If a pH change happens, it will vary by distance from the electrode surface. It has been shown that pH in MRSA infected tissue drops from 7 to 5. This indicates MRSA biofilm cause a pH decrease on the tissue and MRSA can survive at low pH (Wang et al. 2015). In addition, previously, we reported pH changes near working electrode surface measured using a microelectrode and found no significant pH change (Sultana et al. 2015). Lastly, we measured average pH of the hydrogel after 48 hours using a pH paper and it was between 5 and 6.

H_2O_2 transport into the explant is expected to affect biofilm removal and tissue viability. A review of effects of H_2O_2 on the human body found that toxicity can occur at as little as 50 μmol L^{-1}, depending on exposure time and location (Halliwell et al. 2000a; Gülden et al. 2010). During the natural immune response, H_2O_2 is formed from reactive oxygen species and targets bacteria and mammalian cells alike (Halliwell et al. 2000a; Halliwell et al. 2000b). H_2O_2 may contribute to loosening and rupture of tissue fibers, resulting in what appeared to be a crust over the surface of the explants (SI Section 2) (Liu et al. 2014). A reduction in viability in the *ex vivo* porcine explant biofilm model was observed (Fig 6). An important limitation is that *ex vivo* tissue cannot regenerate or protect cells from oxidative stress. Cells are equipped with enzymes such as catalase, glutathione peroxidase, superoxide dismutase and thioredoxin-linked systems to eliminate H_2O_2 and prevent formation of reactive oxygen radicals ($OH^{\cdot}$) (Mahaseth and Kuzminov 2017). In animal models and clinical applications, where the tissue has multiple methods of eliminating H_2O_2, such as using enzymes to prevent formation of $OH^{\cdot}$ and using myeloperoxidase to produce other antimicrobial oxidants, cell viability is expected to be less affected by the e-bandage (Halliwell et al. 2000b; Paumann-Page et al. 2013). Both chemical oxidants and some metabolic products from infections can result in apoptosis and damage to the surrounding tissue of a wound.

A limitation of the *ex vivo* model was the inability to study the impact of the e-bandage on wound healing. Infections are a critical factor impairing wound healing (Guo and Dipietro 2010). Infections alter the balance of inflammation, compete for oxygen, and inhibit the inflammatory phase of wound healing, preventing epithelialization (Armstrong 2021). Documented causes of *S. aureus* causing apoptosis in human tissue and epithelial cells through virulence factor producion support the idea that infections slow or inhibit wound healing. (Haslinger-Löffler et al. 2005; Nakatsuji et al. 2016). *S. aureus* infections also cause alkaline pH and decreased oxygen concentrations at wound surfaces (Lone et al. 2015). Therefore, e-bandage treatment may result in improved wound healing rates due to the removal/reduction of *S. aureus* biofilms.

The results of the *ex vivo* porcine explant biofilm model presented here support that H_2O_2-producing e-bandages slowed down *S. aureus* biofilm colonization and reduced young *S. aureus* biofilms. E-bandage efficacy against mature biofilms was limited. H_2O_2 was shown to penetrate both noninfected and infected explants and e-bandages were shown to reduce eukaryotic cell viability to some extent. Future studies will focus on evaluating the efficacy of the e-bandage in *in vivo* models.

Supplementary Material

Refer to Web version on PubMed Central for supplementary material.

Acknowledgments

Research reported in this publication was supported by the National Institute of Allergy and Infectious Diseases of the National Institutes of Health under award number R01AI091594. The content is solely the responsibility of the authors and does not necessarily represent the official views of the National Institutes of Health. The authors thank C&L Locker in Moscow, ID and the University of Idaho Beef Center for providing the porcine materials. Electron microscopy, sample preparation protocols, and support were provided by the Washington State University Franceschi Microscopy and Imaging Center.

References

Bard Allen J., L.R.F. (2001) Electrochemical Methods: Fundamentals and Applications. New York: Wiley.

Alves DR, Booth SP, Scavone P, Schellenberger P, Salvage J, Dedi C, Thet N-T, Jenkins ATA, Waters R, Ng KW, Overall ADJ, Metcalfe AD, Nzakizwanayo J and Jones BV (2018) Development of a High-Throughput ex-Vivo Burn Wound Model Using Porcine Skin, and Its Application to Evaluate New Approaches to Control Wound Infection. Frontiers in Cellular and Infection Microbiology 8.

Anderl JN, Franklin MJ and Stewart PS (2000) Role of antibiotic penetration limitation in *Klebsiella pneumoniae* biofilm resistance to ampicillin and ciprofloxacin. Antimicrobial agents and chemotherapy 44, 1818–1824. [PubMed: 10858336]

Armstrong DGM, A. J. (2021) Risk factors for impaired wound healing and wound complications ed. Berman RSE, J. F.; Mills JL; Cochran A UpToDate.com.

Cantero D, Cooksley C, Jardeleza C, Bassiouni A, Jones D, Wormald PJ and Vreugde S (2013) A human nasal explant model to study *Staphylococcus aureus* biofilm in vitro. Int Forum Allergy Rhinol 3, 556–562. [PubMed: 23404931]

Davenport EK, Call DR and Beyenal H (2014) Differential Protection from Tobramycin by Extracellular Polymeric Substances from *Acinetobacter baumannii* and *Staphylococcus aureus* Biofilms. Antimicrobial Agents and Chemotherapy 58, 4755–4761. [PubMed: 24913166]

Denkhaus E, Meisen S, Telgheder U and Wingender J (2007) Chemical and physical methods for characterisation of biofilms. Microchimica Acta 158, 1–27.

Devaraj A, Buzzo JR, Mashburn-Warren L, Gloag ES, Novotny LA, Stoodley P, Bakaletz LO and Goodman SD (2019) The extracellular DNA lattice of bacterial biofilms is structurally related to Holliday junction recombination intermediates. Proceedings of the National Academy of Sciences 116, 25068.

Dowd SE, Delton Hanson J, Rees E, Wolcott RD, Zischau AM, Sun Y, White J, Smith DM, Kennedy J and Jones CE (2011) Survey of fungi and yeast in polymicrobial infections in chronic wounds. J Wound Care 20, 40–47. [PubMed: 21278640]

Finnegan M, Linley E, Denyer SP, McDonnell G, Simons C and Maillard JY (2010) Mode of action of hydrogen peroxide and other oxidizing agents: differences between liquid and gas forms. J Antimicrob Chemother 65, 2108–2115. [PubMed: 20713407]

Gülden M, Jess A, Kammann J, Maser E and Seibert H (2010) Cytotoxic potency of H2O2 in cell cultures: impact of cell concentration and exposure time. Free Radic Biol Med 49, 1298–1305. [PubMed: 20673847]

Guo S and Dipietro LA (2010) Factors affecting wound healing. J Dent Res 89, 219–229. [PubMed: 20139336]

Gupta P, Sarkar S, Das B, Bhattacharjee S and Tribedi P (2016) Biofilm, pathogenesis and prevention--a journey to break the wall: a review. Arch Microbiol 198, 1–15. [PubMed: 26377585]

Halliwell B, Clement MV and Long LH (2000a) Hydrogen peroxide in the human body. FEBS Letters 486, 10–13. [PubMed: 11108833]

Halliwell B, Clement MV, Ramalingam J and Long LH (2000b) Hydrogen peroxide. Ubiquitous in cell culture and in vivo? IUBMB Life 50, 251–257. [PubMed: 11327318]

Hampton MB, Kettle AJ and Winterbourn CC (1998) Inside the neutrophil phagosome: oxidants, myeloperoxidase, and bacterial killing. Blood 92, 3007–3017. [PubMed: 9787133]

Haslinger-Löffler B, Kahl BC, Grundmeier M, Strangfeld K, Wagner B, Fischer U, Cheung AL, Peters G, Schulze-Osthoff K and Sinha B (2005) Multiple virulence factors are required for *Staphylococcus aureus*-induced apoptosis in endothelial cells. Cellular Microbiology 7, 1087–1097. [PubMed: 16008576]

Høiby N, Ciofu O, Johansen HK, Song ZJ, Moser C, Jensen P, Molin S, Givskov M, Tolker-Nielsen T and Bjarnsholt T (2011) The clinical impact of bacterial biofilms. Int J Oral Sci 3, 55–65. [PubMed: 21485309]

Jankovskaja S, Labrousse A, Prévaud L, Holmqvist B, Brinte A, Engblom J, Rezeli M, Marko-Varga G and Ruzgas T (2020) Visualisation of H(2)O(2) penetration through skin indicates importance to develop pathway-specific epidermal sensing. Mikrochim Acta 187, 656–656. [PubMed: 33188446]

Kowal J, Tkach M and Théry C (2014) Biogenesis and secretion of exosomes. Curr Opin Cell Biol 29, 116–125. [PubMed: 24959705]

Lewandowski Z and Beyenal H (2013) Fundamentals of Biofilm Research, Second Edition: Taylor & Francis.

Liu X, Jiang Y, He H and Ping W (2014) Hydrogen peroxide-induced degradation of type I collagen fibers of tilapia skin. Food Structure 2, 41–48.

Lone AG, Atci E, Renslow R, Beyenal H, Noh S, Fransson B, Abu-Lail N, Park J-J, Gang DR and Call DR (2015) *Staphylococcus aureus* induces hypoxia and cellular damage in porcine dermal explants. Infect Immun 83, 2531–2541. [PubMed: 25847960]

Mahaseth T and Kuzminov A (2017) Potentiation of hydrogen peroxide toxicity: From catalase inhibition to stable DNA-iron complexes. Mutat Res Rev Mutat Res 773, 274–281. [PubMed: 28927535]

Marquitan M, Clausmeyer J, Actis P, Cordoba AL, Korchev Y, Mark MD, Herlitze S and Schuhmann W (2016) Intracellular Hydrogen Peroxide Detection with Functionalised Nanoelectrodes. Chemelectrochem 3, 2125–2129.

McMahon RE, Salamone AB, Poleon S, Bionda N and Salamone JC (2020) Efficacy of Wound Cleansers on Wound-Specific Organisms Using *In Vitro* and *Ex Vivo* Biofilm Models. Wound Manag Prev 66, 31–42. [PubMed: 33206627]

Metcalf DG and Bowler PG (2013) Biofilm delays wound healing: A review of the evidence. Burns Trauma 1, 5–12. [PubMed: 27574616]

Mohamed A, Anoy MMI, Tibbits G, Raval YS, Flurin L, Greenwood-Quaintance KE, Patel R and Beyenal H (2021) Hydrogen peroxide-producing electrochemical bandage controlled by a wearable potentiostat for treatment of wound infections. Biotechnol Bioeng 118, 2815–2821. [PubMed: 33856049]

Nakatsuji T, Chen TH, Two AM, Chun KA, Narala S, Geha RS, Hata TR and Gallo RL (2016) *Staphylococcus aureus* Exploits Epidermal Barrier Defects in Atopic Dermatitis to Trigger Cytokine Expression. J Invest Dermatol 136, 2192–2200. [PubMed: 27381887]

Ofoedu CE, You L, Osuji CM, Iwouno JO, Kabuo NO, Ojukwu M, Agunwah IM, Chacha JS, Muobike OP, Agunbiade AO, Sardo G, Bono G, Okpala COR and Korzeniowska M (2021) Hydrogen Peroxide Effects on Natural-Sourced Polysacchrides: Free Radical Formation/Production, Degradation Process, and Reaction Mechanism-A Critical Synopsis. Foods 10.

Paumann-Page M, Furtmüller PG, Hofbauer S, Paton LN, Obinger C and Kettle AJ (2013) Inactivation of human myeloperoxidase by hydrogen peroxide. Arch Biochem Biophys 539, 51–62. [PubMed: 24035742]

Percival SL, Hill KE, Williams DW, Hooper SJ, Thomas DW and Costerton JW (2012) A review of the scientific evidence for biofilms in wounds. Wound Repair Regen 20, 647–657. [PubMed: 22985037]

Phillips PL, Yang Q, Davis S, Sampson EM, Azeke JI, Hamad A and Schultz GS (2015) Antimicrobial dressing efficacy against mature Pseudomonas aeruginosa biofilm on porcine skin explants. Int Wound J 12, 469–483. [PubMed: 24028432]

Raval YS, Flurin L, Mohamed A, Greenwood-Quaintance KE, Beyenal H and Patel R (2021a) *In Vitro* Antibacterial Activity of Hydrogen Peroxide and Hypochlorous Acid, Including That Generated by Electrochemical Scaffolds. Antimicrobial Agents and Chemotherapy 65, e01966–01920.

Raval YS, Mohamed A, Flurin L, Mandrekar JN, Greenwood Quaintance KE, Beyenal H and Patel R (2021b) Hydrogen-peroxide generating electrochemical bandage is active in vitro against mono- and dual-species biofilms. Biofilm 3, 100055. [PubMed: 34585138]

Raval YS, Mohamed A, Mandrekar JN, Fisher C, Greenwood-Quaintance KE, Beyenal H and Patel R (2022) In Vitro Antibiofilm Activity of Hydrogen Peroxide-Generating Electrochemical Bandage against Yeast Biofilms. Antimicrob Agents Chemother 66, e0179221. [PubMed: 34930030]

Raval YS, Mohamed A, Song J, Greenwood-Quaintance KE, Beyenal H and Patel R (2020) Hydrogen Peroxide-Generating Electrochemical Scaffold Activity against Trispecies Biofilms. Antimicrobial Agents and Chemotherapy 64, e02332–02319. [PubMed: 31964793]

Raval YS, Mohamed A, Zmuda HM, Patel R and Beyenal H (2019) Hydrogen-Peroxide-Generating Electrochemical Scaffold Eradicates Methicillin-Resistant Staphylococcus aureus Biofilms. Global Challenges 3, 1800101. [PubMed: 31218078]

Roberts AEL, Powell LC, Pritchard MF, Thomas DW and Jenkins RE (2019) Anti-pseudomonad Activity of Manuka Honey and Antibiotics in a Specialized *ex vivo* Model Simulating Cystic Fibrosis Lung Infection. Front Microbiol 10, 869. [PubMed: 31105667]

Roche ED, Woodmansey EJ, Yang Q, Gibson DJ, Zhang H and Schultz GS (2019) Cadexomer iodine effectively reduces bacterial biofilm in porcine wounds *ex vivo* and *in vivo*. Int Wound J 16, 674–683. [PubMed: 30868761]

Sen CK (2019) Human Wounds and Its Burden: An Updated Compendium of Estimates. Adv Wound Care (New Rochelle) 8, 39–48. [PubMed: 30809421]

Shrout JD, Tolker-Nielsen T, Givskov M and Parsek MR (2011) The contribution of cell-cell signaling and motility to bacterial biofilm formation. MRS Bull 36, 367–373. [PubMed: 22053126]

Stewart PS (1996) Theoretical aspects of antibiotic diffusion into microbial biofilms. Antimicrobial Agents and Chemotherapy 40, 2517–2522. [PubMed: 8913456]

Stewart PS, Roe F, Rayner J, Elkins JG, Lewandowski Z, Ochsner UA and Hassett DJ (2000) Effect of catalase on hydrogen peroxide penetration into Pseudomonas aeruginosa biofilms. Applied and Environmental Microbiology 66, 836–838. [PubMed: 10653761]

Sullivan TP, Eaglstein WH, Davis SC and Mertz P (2001) The pig as a model for human wound healing. Wound Repair Regen 9, 66–76. [PubMed: 11350644]

Sultana ST, Atci E, Babauta JT, Mohamed Falghoush A, Snekvik KR, Call DR and Beyenal H (2015) Electrochemical scaffold generates localized, low concentration of hydrogen peroxide that inhibits bacterial pathogens and biofilms. Scientific Reports 5, 14908. [PubMed: 26464174]

Sultana ST, Call DR and Beyenal H (2016) Eradication of *Pseudomonas aeruginosa* biofilms and persister cells using an electrochemical scaffold and enhanced antibiotic susceptibility. npj Biofilms and Microbiomes 2, 2. [PubMed: 28649396]

Uruen C, Chopo-Escuin G, Tommassen J, Mainar-Jaime RC and Arenas J (2021) Biofilms as Promoters of Bacterial Antibiotic Resistance and Tolerance. Antibiotics (Basel) 10, 3.

Valadi H, Ekström K, Bossios A, Sjöstrand M, Lee JJ and Lötvall JO (2007) Exosome-mediated transfer of mRNAs and microRNAs is a novel mechanism of genetic exchange between cells. Nat Cell Biol 9, 654–659. [PubMed: 17486113]

Wang F, Raval Y, Tzeng T-RJ and Anker JN (2015) X-Ray Excited Luminescence Chemical Imaging of Bacterial Growth on Surfaces Implanted in Tissue. Advanced Healthcare Materials 4, 903–910. [PubMed: 25611007]

Yang Q, Larose C, Della Porta AC, Schultz GS and Gibson DJ (2017) A surfactant-based wound dressing can reduce bacterial biofilms in a porcine skin explant model. Int Wound J 14, 408–413. [PubMed: 27212453]

Yang Q, Phillips PL, Sampson EM, Progulske-Fox A, Jin S, Antonelli P and Schultz GS (2013) Development of a novel ex vivo porcine skin explant model for the assessment of mature bacterial biofilms. Wound Repair Regen 21, 704–714. [PubMed: 23927831]

Yik-Sham Chung C, Timblin GA, Saijo K and Chang CJ (2018) Versatile Histochemical Approach to Detection of Hydrogen Peroxide in Cells and Tissues Based on Puromycin Staining. Journal of the American Chemical Society 140, 6109–6121. [PubMed: 29722974]

Zmuda HM, Mohamed A, Raval YS, Call DR, Schuetz AN, Patel R and Beyenal H (2020) Hypochlorous acid-generating electrochemical scaffold eliminates *Candida albicans* biofilms. Journal of Applied Microbiology 129, 776–786. [PubMed: 32249986]

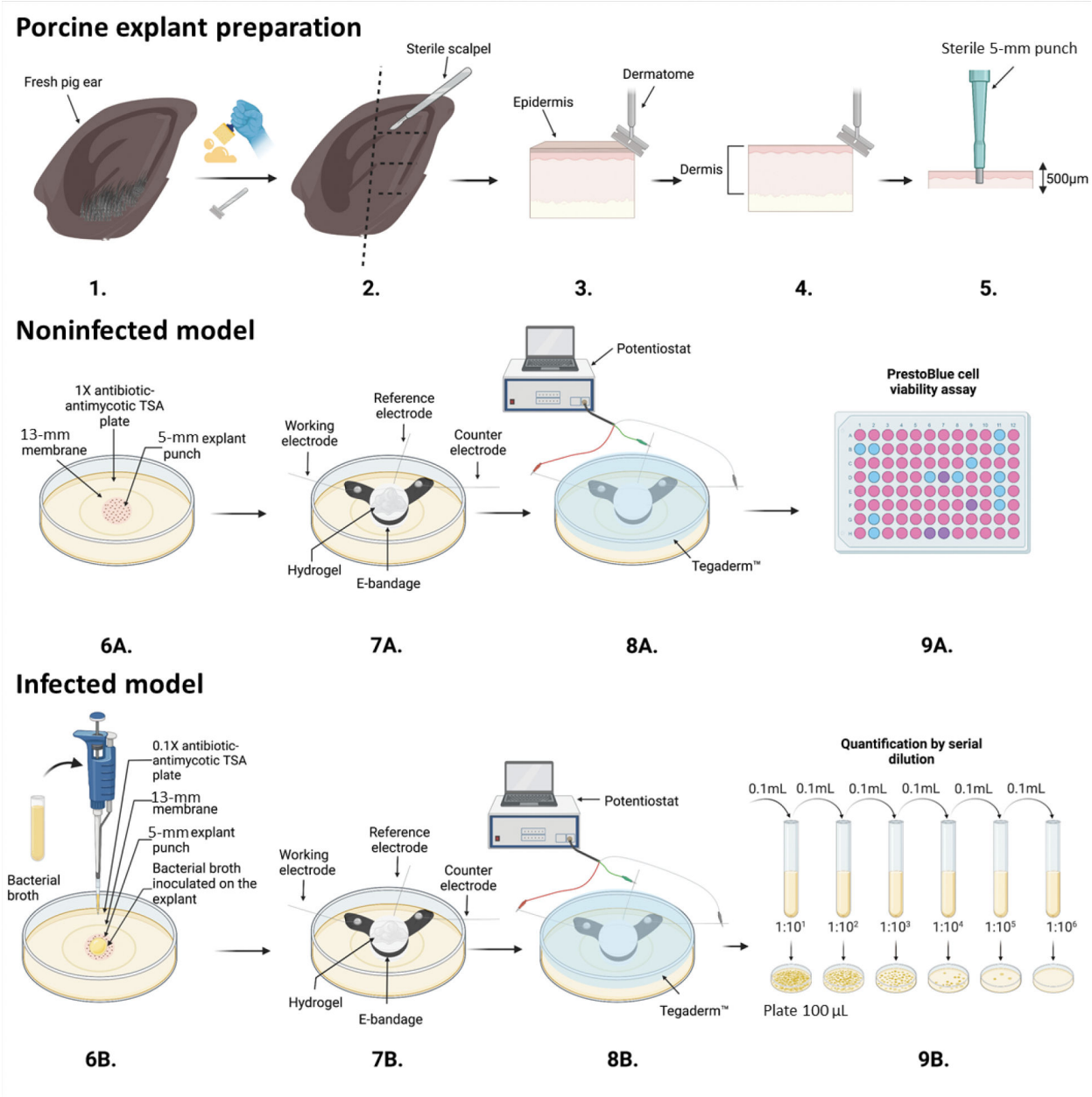

Figure 1.

Schematic of porcine explant preparation (1–5), noninfected model (6A–9A), and infected model experiments (6B–9B), e-bandage applications and treatment (7A, 8A, 7B, 8B), colony-forming unit quantification (9B), and Prestoblue cell viability assay (9A). Images prepared using BioRender©.

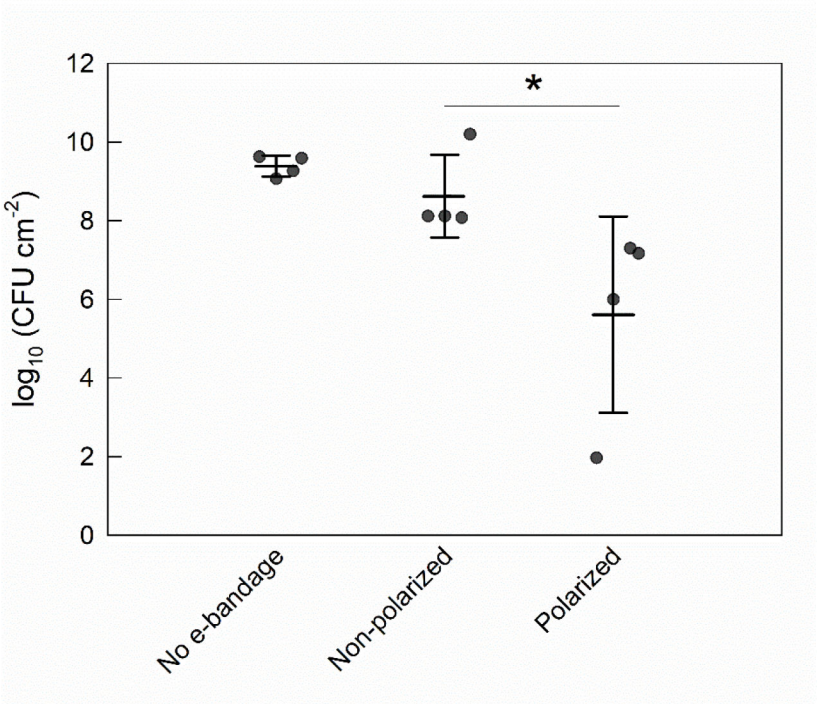

Figure 2.

Effect of the e-bandage on porcine explant colonization by *S. aureus*. Treatment started immediately following explant inoculation with *S. aureus.* Data points represent individual replicates (circles), averages (horizontal lines) and standard deviations of treatment conditions. Statistical significance is indicated by a star (n = 4).

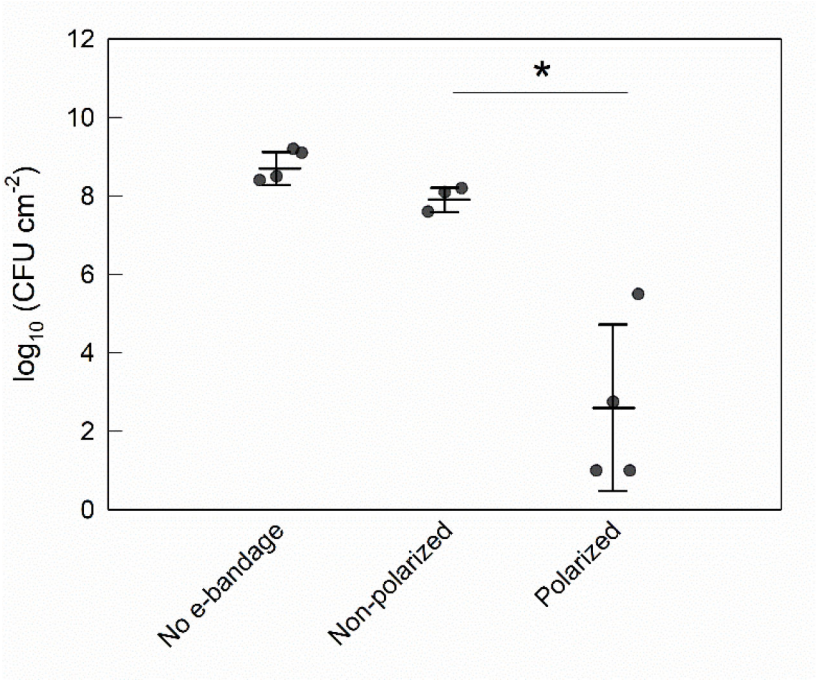

Figure 3.

Colony-forming units of *S. aureus* biofilms grown on porcine explants after treatment with the e-bandage for biofilm removal of young biofilms. Treatment started 24 h after explant inoculation with *S. aureus.* Data points represent individual replicates (circles), averages (horizontal lines) and standard deviations of treatment conditions. Statistical significance is indicated by a star (n = 4).

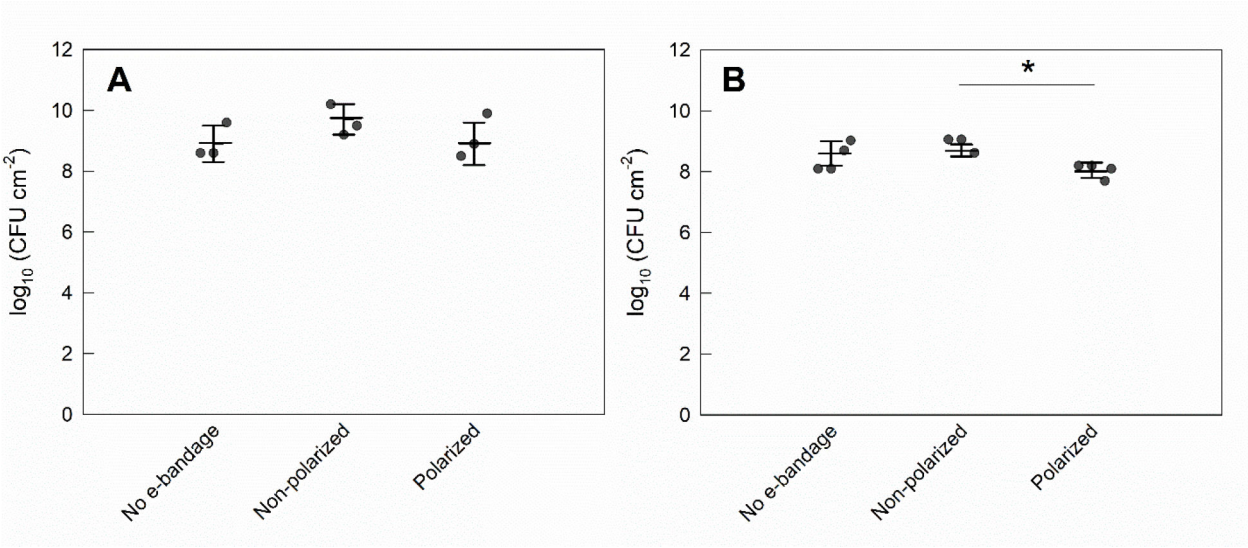

Figure 4.

Colony-forming units of *S. aureus* biofilms grown on pig ear explants after treatment with the e-bandages. Treatment started 3 days after explant inoculation with *S. aureus* inoculum of A) 10 μl and B) 2.5 μl. Data points represent individual replicates (circles), averages (horizontal lines) and standard deviations of treatment conditions. Statistical significance is indicated by a star (n ≥3).

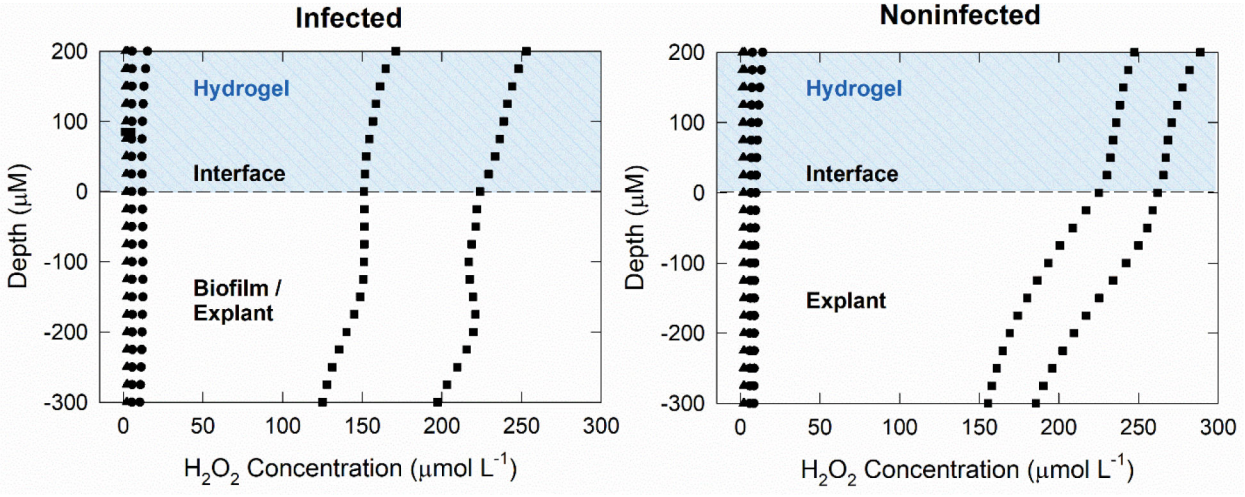

Figure 5.

Depth profiles of the concentration of H_2O_2 generated by polarized e-bandages in explant tissue and overlying hydrogel: A) infected and B) noninfected explants.

▲ explant at baseline with no treatment; ● explant after exposure to non-polarized e-bandage for 48 h; and ■ explant exposed to a polarized e-bandage for 48 h.

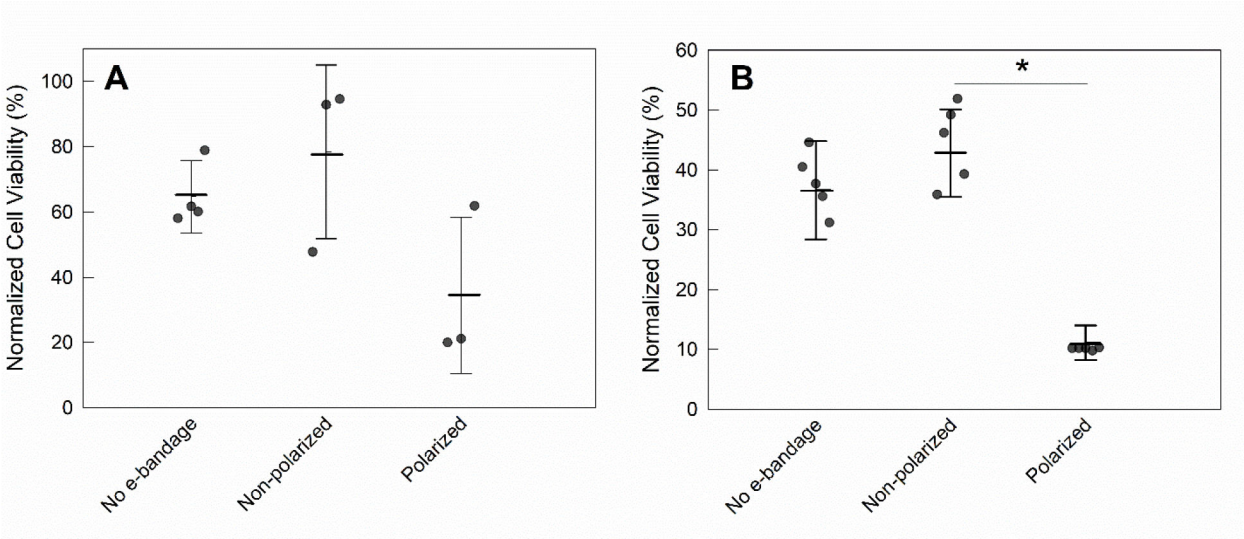

Figure 6.

Effect of e-bandage on cell viability of noninfected explants. Normalized cell viability of explants treated with no e-bandage, or non-polarized or polarized e-bandages at A) t = 0 and B) t = 3 days. Data points represent individual replicates (circles), averages (horizontal lines) and standard deviations of treatment conditions. Statistical significance is indicated by a star ($n \geq 3$).